



Title	In situ precipitation of amorphous calcium phosphate nanoparticles within 3D porous collagen sponges for bone tissue engineering
Author(s)	Santhakumar, Syama; Oyane, Ayako; Nakamura, Maki et al.
Citation	Materials Science and Engineering: C, 116, 111194 https://doi.org/10.1016/j.msec.2020.111194
Issue Date	2020-11
Doc URL	https://hdl.handle.net/2115/87263
Rights	© 2020. This manuscript version is made available under the CC-BY-NC-ND 4.0 license http://creativecommons.org/licenses/by-nc-nd/4.0/
Rights(URL)	https://creativecommons.org/licenses/by-nc-nd/4.0/
Type	journal article
File Information	Syama_Mater Sci Eng C_2020.pdf



***In situ* precipitation of amorphous calcium phosphate nanoparticles within 3D porous collagen sponges for bone tissue engineering**

**Syama Santhakumar,^{1*} Ayako Oyane,^{1*} Maki Nakamura,¹ Kenji Koga,¹ Saori Miyata,²
Ko Muratsubaki,² Hirofumi Miyaji²**

¹ Nanomaterials Research Institute, National Institute of Advanced Industrial Science and Technology (AIST), Central 5, 1-1-1 Higashi, Tsukuba, Ibaraki, 305-8565, Japan

² Department of Periodontology and Endodontology, Faculty of Dental Medicine, Hokkaido University, N13W7, Kita-ku, Sapporo, Hokkaido, 060-8586, Japan

* Corresponding author: **Ayako Oyane**, PhD, **Syama Santhakumar**, PhD

Nanomaterials Research Institute, National Institute of Advanced Industrial Science and Technology (AIST)

E-mail: a-oyane@aist.go.jp, syama-santhakumar@aist.go.jp, Tel: +81-29-861-3005,

Fax: +81-29-861-3005

Address: Central 5, 1-1-1 Higashi, Tsukuba, Ibaraki, 305-8565, Japan

Abstract

Amorphous calcium phosphate (ACP) plays an important role in biomineralization within the three-dimensional (3D) collagen network in human hard tissues, and exhibits osteoconductivity. Porous collagen sponges coated with ACP nanoparticles could be considered as potential scaffolds for use in bone tissue engineering. In this study, such composite materials were fabricated *via* homogeneous ACP precipitation using a supersaturated calcium phosphate (CaP) solution. Homogeneous ACP precipitation was induced *in situ* within the sponges by a temperature-controlled coating process composed of two steps. In the first step, the CaP solution was cooled to 4 °C to suppress precipitation until the solution penetrated fully into the sponge's internal pores. In the second step, the CaP solution was warmed up to 25 °C with continuous shaking to induce ACP precipitation within the sponges. The resulting sponges were therefore coated with ACP nanoparticles on their inner and outer surfaces. A simulated body fluid (SBF) test indicated osteoconductivity of the collagen sponges coated with ACP nanoparticles. Further, ACP-coated collagen sponges immobilizing basic fibroblast growth factor (bFGF) were fabricated using the CaP solution supplemented with bFGF. The fabricated sponges allowed the sustained release of bFGF in a culture medium and enhanced proliferation of osteoblastic MC3T3-E1 cells. Such ACP-coated collagen sponges have the potential to be used as scaffolds in bone tissue engineering if pursued for further *in vitro* and *in vivo* studies.

Key words: amorphous calcium phosphate (ACP), nanoparticles, scaffold, bone tissue engineering, basic fibroblast growth factor (bFGF), nucleation

1. Introduction

Bone has a complex structure that is made up primarily of three-dimensional (3D) assembled organic collagen fibers infused with calcium phosphate (CaP) crystals (mainly low-crystalline apatite) and bone cells. Bone tissue engineering requires scaffolds that can provide suitable environment for new bone formation. An ideal scaffold for bone tissue engineering should have a 3D porous structure to allow cell infiltration, possess biocompatible and osteogenic properties, and be biodegradable and bioresorbable in the body to be replaced with newly formed bone tissue [1]. Atelocollagen has been widely used as a scaffold material for tissue engineering owing to its biodegradable, bioresorbable, and biocompatible nature, along with low antigenicity [2]. Various techniques to combine collagen-based materials with CaPs have been proposed to improve the mechanical and osteogenic properties for bone tissue engineering [3-14]. For example, precipitation processes [3-7, 9, 11, 13, 14], mixing of CaP granules [12] and infiltration of CaP nanoparticles [8, 10] have been proposed to fabricate CaP-collagen composites. Most of the previous studies cited above refer to the use of crystalline CaPs, such as brushite [3], apatite [4, 6, 7, 9, 11], β -tricalcium phosphate (β -TCP) [8, 10, 12], and octacalcium phosphate (OCP) [5, 12]. However, few attempts have been made to combine collagen-based materials with amorphous calcium phosphate (ACP) [13, 14].

ACP plays an important role in biomineralization in humans [15] and shows excellent biological properties such as osteoconductivity [16-18], better cell attachment [19, 20], osteoinductivity [21-23], and biodegradability [24, 25] as compared to crystalline apatite. Numerous *in vitro* [26-28] and *in vivo* [29, 30] evidences suggest that biomineralization, *i.e.*, *in vivo* bone apatite formation, occurs through an intermediate amorphous phase that later transforms into crystalline apatite. This reaction occurs spontaneously because crystalline apatite is thermodynamically the most stable phase among all the CaP phases under body environmental conditions [31]. It has been reported that disordered (amorphous) CaP

nanoparticles (50–80 nm in diameter) formed within osteoblasts are transported to an extracellular space and are crystallized into apatite on the collagen fibrils [27, 32]. Coating of the surface of a 3D porous collagen sponge with ACP nanoparticles would result in the formation of a composite resembling the bone matrix structure at the initial stage of biomineralization. This type of ACP-collagen composites might be novel and highly functional scaffolds for bone tissue engineering. There are several reports about ACP-polymer composites including ACP-collagen [13, 14], ACP-poly(L-lactic acid) [33], ACP-poly(lactide-co-glycolide) [34], and ACP-carboxymethyl chitosan [35]. However, there has been little attempt to fabricate 3D porous sponges coated with ACP on their inner as well as outer surfaces.

The main purpose of the present study was to fabricate 3D porous collagen sponges coated with ACP nanoparticles on their inner and outer surfaces through *in situ* ACP precipitation within the sponges. ACP nanoparticles are known to be fabricated easily *via* homogeneous CaP nucleation (amorphous phase nucleation) in highly supersaturated labile CaP solutions. In our previous studies, a dense polymer substrate was coated with ACP nanoparticles utilizing a labile CaP solution [36, 37]. These studies reported that ACP nanoparticles formed promptly in the CaP solution upon mixing source Ca and P solutions, and deposited onto the substrate *via* gravity sedimentation. In the present study, a temperature-controlled ACP coating process *via in situ* precipitation within the sponges was proposed to coat the inner and outer surfaces of 3D porous sponges with ACP nanoparticles. This was achieved by suppressing CaP precipitation until the supersaturated CaP solution penetrated fully into the internal pores of the sponge by cooling the solution.

Calf dermal-derived type I and III atelocollagen sponges that have been in clinical use as wound dressings and bone cartilage substitutes were used as 3D porous collagen sponges. The uncoated and ACP-coated sponges were analyzed on their inner and outer surfaces. As a

preliminary osteoconductivity assay, their apatite-forming ability was examined using a simulated body fluid (SBF) [38]. Additionally, to demonstrate the potential for further improvement of the sponge's biological function, we carried out the same coating process using the CaP solution supplemented with basic fibroblast growth factor (bFGF) to fabricate ACP-collagen composites with bFGF-release capability. bFGF is a cytokine that can enhance proliferation and differentiation of various cell types, and thus, regeneration of soft and hard tissues [39].

2. Materials and Methods

2.1. Preparation of the sponges

A sterile sponge sheet of calf dermal-derived type I and III atelocollagen (Terudermis) was purchased from Olympus Terumo Biomaterials Corp., Japan. This sponge sheet has a 3D porous structure with the pore-size and longer pore diameter of $14956 \pm 2710 \mu\text{m}^2$ and $178.1 \pm 53.9 \mu\text{m}$, respectively [40]. The sponge sheet was cut into cubic blocks ($1 \text{ mm} \times 1 \text{ mm} \times 1 \text{ mm}$). The sponges (referred to as Col) were kept at $-80 \text{ }^\circ\text{C}$ until further use.

2.2. Temperature-controlled ACP coating process

Before the coating process, we prepared sterile six source solutions: (1) 12.5 mM CaCl_2 solution, (2) 25 mM $\text{K}_2\text{HPO}_4 \cdot 3\text{H}_2\text{O}$ solution, (3) 710 mM NaCl solution, (4) 300 mM NaHCO_3 solution, (5) physiological saline containing 20 $\mu\text{g}/\text{mL}$ bFGF, and (6) physiological saline. The physiological saline used was a clinically approved one (Otsuka Normal Saline TN, Otsuka Pharmaceutical Co., Ltd., Japan) comprising of 154 mM NaCl solution. The bFGF-containing physiological saline was prepared aseptically by dissolving pharmaceutical human-recombinant bFGF (Fiblast[®], Kaken Pharmaceutical Co., Ltd., Japan) in the clinically approved

physiological saline. Other source solutions (1)–(4) were prepared by dissolving reagent grade chemicals (all from Nacalai Tesque, Inc., Japan) in ultrapure water and sterilized using a 0.22 μm pore-sized membrane filter. All these source solutions were kept at 4 °C for at least 30 min in a dry bath incubator (H2O3-PRO, Coyote Bioscience Co., Ltd., China) before use in the coating process.

The Col sponges were subjected to the temperature-controlled ACP coating process composed of two steps: 1st immersion step at 4 °C and 2nd immersion step at 25 °C. In this process, two types of supersaturated CaP solutions (5.0 mM CaCl_2 , 2.5 mM $\text{K}_2\text{HPO}_4 \cdot 3\text{H}_2\text{O}$, 172.8 mM NaCl , and 30.0 mM NaHCO_3) with and without bFGF (4 $\mu\text{g}/\text{mL}$) were prepared under aseptic conditions using the previously prepared six source solutions. The Ca and P concentrations of the supersaturated CaP solutions were almost equivalent to those of the CaP solution used in our previous study (5.15 mM Ca^{2+} , 2.57 mM $\text{H}_2\text{PO}_4^-/\text{HPO}_4^{2-}$, and 15.15 mM HCO_3^-) [37, 41]. In this study, the NaHCO_3 concentration was doubled and vent-cap tubes were employed to enhance carbonate degassing from the CaP solutions and the resulting pH increase during the 2nd immersion step at 25 °C.

Just before the coating process, the Col sponges were treated with oxygen plasma in order to increase their surface wettability. In the plasma treatment, the sponges were exposed to O_2 gas plasma at a power density of 0.1 W/cm^2 and a pressure of 30 Pa under an electric field operating at 13.56 MHz for 30 s using a compact ion etcher (FA-1, Samco Inc., Japan). The plasma-treated sponges were subjected to the coating process under aseptic conditions. First, 2.0 mL of the CaCl_2 solution and 1.0 mL of the NaCl solution were mixed in a vent-cap tube at 4 °C in the dry bath incubator. The plasma-treated sponges (4 mg per tube) were transferred into the mixed solution (3.0 mL) and degassed for about 30 min at room temperature using a vacuum desiccator (Type VS, AS ONE Corporation, Japan). Following degassing, the solution containing the sponges was cooled again to 4 °C by incubating for 10–15 min in the

dry bath incubator. Meanwhile, the $K_2HPO_4 \cdot 3H_2O$ solution, the $NaHCO_3$ solution, and the physiological saline with or without bFGF were mixed in volume ratio of 1 : 1 : 2 in another tube at 4 °C in the dry bath incubator. 2 mL of the mixed solution was added drop wise to the cooled solution (in the vent-cap tube) containing the sponges under gentle vortexing to prepare the supersaturated CaP solution with or without bFGF (1st immersion step). The CaP solutions containing the sponges were then incubated at 25 °C under orbital shaking (70 r/min) using a shaking incubator (DWMax M-BR-104P, TAITEC Co., Ltd., Japan) for 24 h (2nd immersion step). After incubation, the sponges were washed thrice with ultrapure water and frozen at -80 °C in a deep-freezer for 24 h. The sponges were then freeze-dried using a freeze dryer (EYELA FDS-1000, Tokyo Rikakikai Co., Ltd., Japan), and stored at -20 °C before further analyses. The resulting sponges prepared using the CaP solution with or without bFGF were referred to as F-CaP-Col and CaP-Col, respectively.

2.3. Analyses of the CaP solution

The CaP solution (5 mL) with neither bFGF nor the Col sponges was prepared in the vent-cap tube *via* the same protocol as described in Section 2.2 to study its stability and pH change with time. The same CaP solution (no bFGF, no Col sponges) was prepared at 25 °C by setting the temperature of the dry bath incubator at 25 °C for comparison. The transparency of the CaP solutions just after preparation at 4 °C and 25 °C was examined by visual inspection. The stability of the CaP solution prepared at 4 °C was further analyzed by laser inspection. The CaP solution prepared at 4 °C was kept at 4 °C without shaking or transferred to the shaking incubator (70 r/min) set at 25 °C. After keeping the solution for various periods up to 30 min, laser inspection was performed to check if colloidal CaP particles exist in the solution (this was judged by Tyndall scattering from the particles). In the laser inspection, continuous laser beam (532 nm, < 1 mW) was irradiated to the solution with a laser pointer (LP-GL1001, SANWA

SUPPLY INC., Japan). The distance between the laser pointer and the side of the tube was approximately 8 cm. Appearance of the CaP solution under laser irradiation was captured using a digital camera (Tough TG-5, Olympus Corporation, Japan). The pH of the CaP solution just after preparation at 4 °C and that after incubation for 24 h at 4 °C (without shaking) and 25 °C (under shaking at 70 r/min) was measured using a pH Meter (D-71, Horiba, Ltd., Japan). Three independent tubes were used for each measurement to obtain mean \pm standard deviation (SD).

2.4. Surface analyses

The sponges obtained in Sections 2.2 were analyzed using a tabletop scanning electron microscope (SEM; TM4000Plus, Hitachi High-Tech Fielding Corporation, Japan), field emission SEM (FESEM; S-4800, Hitachi High-technologies Corporation, Japan) equipped with an energy dispersive X-ray (EDX) spectrometer (EMAX X-act, Horiba, Ltd., Japan), a Fourier transform infrared (FT-IR) spectrometer (FT/IR-4700, JASCO Corporation, Japan), and an X-ray diffraction (XRD) analyzer (M18X, MacScience, Japan). Preceding the FESEM and EDX analyses, the inner surfaces of the sponges were exposed by cutting them into two halves using a microtome blade (Feather S35, Feather Safety Razor Co., Ltd., Japan). The sponges were fixed on a metallic sample holder with adhesive carbon tape, coated with carbon using a carbon coater (VC-100S/100W, Vacuum device Co., Ltd., Japan), and used for the SEM, FESEM, and EDX analyses. The SEM analysis was performed with the backscattered electron (BSE) mode at an accelerating voltage of 15.0 kV. The FESEM and EDX analyses were performed with the secondary electron (SE) mode at an accelerating voltage of 15.0 kV, an emission current of 10 μ A, and a working distance of approximately 15 mm. The FT-IR measurements were carried out using an attenuated total reflection (ATR) accessory with a monolithic diamond crystal at a resolution of 4 cm^{-1} with a total of 80 scans. The XRD measurements were performed with $\text{CuK}\alpha$ radiation ($\lambda = 0.154178$ nm) at 40 kV and 200 mA

with the thin-film mode at an incidence angle of 1° , a 2θ step width of 0.05° , and a counting time of 6 s per step for the sponges (4 mg) fixed on a silicon sample holder with adhesive polyimide tape.

2.5. Cross-sectional analyses

Cross-sectional analyses were carried out for the CaP-Col sponges by a conventional resin embedding method. First, the CaP-Col sponges were embedded in an epoxy resin and cured at 60°C . Cross-sectional ultra-thin specimens, approximately 150 nm in thickness were prepared from the cured resin under the dry condition using an ultramicrotome. The ultra-thin specimens were analyzed using an analytical transmission electron microscope (TEM; Tecnai Osiris, FEI, USA) operated at 200 kV equipped with an energy dispersive X-ray spectrometer (EDX; Super-X system, FEI, USA) and a high-angle annular dark-field scanning TEM (HAADF-STEM) system with a probe diameter of approximately 1 nm. Crystalline structures of the specimens were examined by selected area electron diffraction (SAED) analyses.

2.6. Simulated body fluid (SBF) test

As a preliminary osteoconductivity assay, SBF test was carried out for the CaP-Col sponges according to ISO23317. SBF (so-called c-SBF: 142.0 mM Na^{2+} , 5.0 mM K^+ , 1.5 mM Mg^{2+} , 2.5 mM Ca^{2+} , 147.8 mM Cl^- , 4.2 mM HCO_3^- , 1.0 mM HPO_4^{2-} , 0.5 mM SO_4^{2-}) was prepared by dissolving reagent-grade chemicals: NaCl, NaHCO_3 , KCl, $\text{K}_2\text{HPO}_4 \cdot 3\text{H}_2\text{O}$, $\text{MgCl}_2 \cdot 6\text{H}_2\text{O}$, CaCl_2 , and Na_2SO_4 into ultrapure water and buffering the solution to $\text{pH} = 7.40$ at 36.5°C with 50 mM tris(hydroxymethyl)aminomethane and HCl as per the protocol described elsewhere [38]. The sponges (4 mg) of CaP-Col and Col as a control were immersed in 30 mL of SBF at 36.5°C for 7 d. After 7 d, the sponges were washed thrice with ultrapure water, and freeze-dried. Surface structures of the sponges were examined with FESEM and

XRD analyzer under the same conditions as described in Section 2.4 to examine the apatite-forming ability of the sponges.

2.7. In vitro bFGF-release assay

Release profile of bFGF from the F-CaP-Col sponges was studied in a serum-free medium (Gibco™ MEM α ; nucleosides, GlutaMAX™, Thermo Fisher Scientific, USA). First, the F-CaP-Col sponges (4 mg) were transferred into 200 μ L of the medium in each well of a 48-well plate. The sponges were degassed for about 30 min using the vacuum desiccator to immerse them completely in the medium. Following the degassing, 300 μ L of the medium was added to each well to increase the medium volume up to a total of 500 μ L. The sponges immersed in the medium were then incubated in a humidified atmosphere containing 5% CO₂ at 37 °C. Pre- and post-incubation for 1, 3, and 7 d, 10 μ L of the medium was sampled from each well, and stored at -80 °C until enzyme linked immunosorbent assay (ELISA) was performed. The sampled medium was assayed for bFGF using an ELISA kit (Human FGF basic Quantikine ELISA kit, R&D systems, Inc., USA).

2.8. In vitro cell proliferation assay

The biological effect of bFGF immobilized on the F-CaP-Col sponges was examined with cell proliferation assay using the CaP-Col sponges as a control. Mouse osteoblastic MC3T3-E1 cells (RIKEN BioResource Research Center, Japan) were cultured using the serum-free medium (Gibco™ MEM α ; nucleosides, GlutaMAX™, Thermo Fisher Scientific, USA) supplemented with 1% antibiotic (Gibco™ penicillin–streptomycin (10,000 U/mL), Thermo Fisher Scientific, USA) in the presence of the sponges. First, the Col, CaP-Col, or F-CaP-Col sponges (4 mg) were transferred into 200 μ L of the medium in each well of a 48-well plate and degassed for about 30 min using the vacuum desiccator to immerse the sponges

completely in the medium. Following the degassing, 300 μL of the cell suspension (1×10^4 cells/well) was added to each well. The cells were incubated in a humidified atmosphere containing 5% CO_2 at 37 $^\circ\text{C}$ for up to 7 d. Following the incubation, the relative number of cells in each well was quantified with water-soluble tetrazolium salt-8 using a cell counting kit (CCK-8, Dojindo Laboratories, Japan), in accordance with the manufacturer's instructions. The absorbance was measured at 450 nm using a microplate reader (MultiskanTM FC, Thermo Fisher Scientific, USA).

2.9. Statistical Analysis

The *in vitro* bFGF-release assay (Section 2.7) and *in vitro* cell proliferation assay (Section 2.8) were carried out in 3 and 6 independent wells, respectively. The obtained experimental values were presented as mean \pm SD. All the statistical analyses were performed using Student's t-test, and $p < 0.05$ was considered statistically significant.

3. Results and discussion

3.1. Analyses of the CaP solution

In our temperature-controlled ACP coating process, the plasma-treated sponges were immersed fully in a cooled (4 $^\circ\text{C}$) supersaturated CaP solution (1st immersion step) which was then kept at an elevated temperature of 25 $^\circ\text{C}$ with continuous shaking for 24 h (2nd immersion step) (figure 1). It was hypothesized that the increase in solution temperature from 4 to 25 $^\circ\text{C}$ should be a cue to induce CaP precipitation by increasing the mass transfer rate along with the degree of supersaturation of the solution *via* carbonate degassing and the resulting pH increase. To verify this hypothesis, the stability and pH change with time of the bFGF-free supersaturated CaP solution without sponges was examined at 4 $^\circ\text{C}$ and 25 $^\circ\text{C}$.

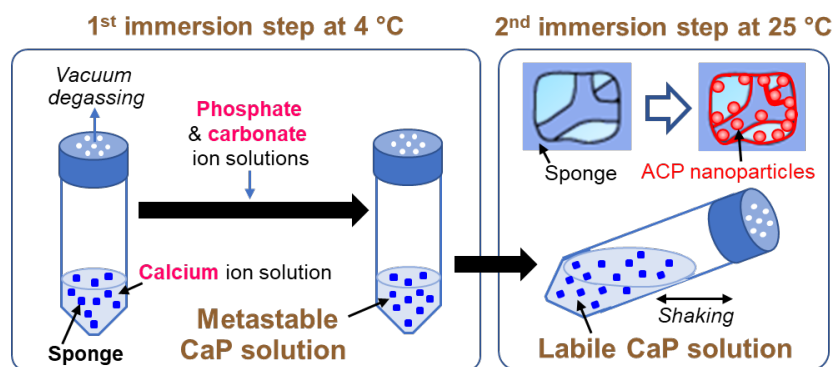


Figure 1. Schematic representation of the temperature-controlled ACP coating process. The 1st immersion step allows penetration of the metastable CaP solution within the sponges. The 2nd immersion step allows ACP coating on the inner and outer surfaces of the sponges *via* homogenous CaP precipitation within the sponges.

The hypothesis described above was supported experimentally; the induction time for CaP precipitation in the supersaturated CaP solution was longer at 4 °C than at 25 °C. According to the visual inspection, the CaP solution prepared at 25 °C showed white turbidity within a few minutes after mixing the source solutions. This phenomenon indicates that the CaP solution induced homogeneous CaP precipitation immediately after preparation at 25 °C, which agrees with some previous reports of a similarly prepared CaP solution [37, 41]. On the other hand, the CaP solution prepared at 4 °C (the same condition as the 1st immersion step) was colorless and transparent just after preparation in the visual inspection (figure 2(a)). This CaP solution (prepared at 4 °C) was kept at 4 °C without shaking or transferred to a shaking incubator kept at 25 °C, and then subjected to the laser inspection. The CaP solution was kept transparent for 10 min at 4 °C without inducing precipitation and induced homogeneous CaP precipitation only after 15 min (figure 2(b), upper row). The homogeneous CaP precipitation after 15 min was evident from the laser beam path (horizontal green line) visualized due to

Tyndall scattering by colloidal particles in the solution. When the same CaP solution (prepared at 4 °C) was transferred to a shaking incubator kept at 25 °C, the solution was heated quickly (raised to 16 ± 0.3 °C by 5 min) and this induced homogeneous CaP precipitation within 5 min (figure 2(b), lower row). These results suggest that the supersaturated CaP solution is labile at 25 °C and induces homogeneous CaP precipitation promptly, whereas the metastability could be maintained at 4 °C within an incubation period of about 10 min.

The pH values of the CaP solution prepared at 4 °C and that of the solution after 24 h incubation at 4 °C were 8.39 ± 0.09 and 8.51 ± 0.06 , respectively, showing that the pH change was not significant at the tested condition at 4 °C. On the other hand, a significant increase in pH (9.42 ± 0.01) was noticed after shaking incubation for 24 h at 25 °C (the same condition as the 2nd immersion step).

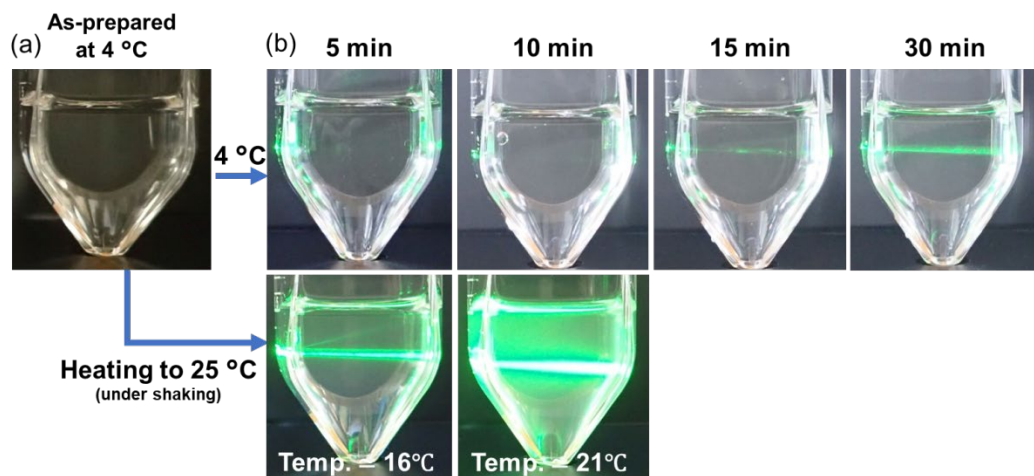


Figure 2. Digital camera images of the CaP solutions, (a) just after preparation at 4 °C, and (b) prepared at 4 °C and then kept at 4 °C (upper row) or transferred to a shaking incubator set at 25 °C (lower row) for various periods up to 30 min. Laser beam was irradiated to the CaP solutions in (b) to visualize CaP formation from Tyndall scattering from colloidal particles (observed as green lines) in the solutions. The CaP solution prepared at 4 °C (a) induced

precipitation after 10–15 min, which was shortened to less than 5 min when heated to 25 °C (b).

3.2. Surface and cross-sectional analyses

Spherical CaP nanoparticles, 200–500 nm in diameter, formed on both the inner and outer surfaces of the CaP-Col and F-CaP-Col sponges without spoiling the porous structure of the sponges. As shown in the whole picture (figure 3(a)), the untreated Col sponges had a large number of pores with the diameter of a few hundred micrometers, in agreement with a previous report [40]. This highly porous structure of the sponge was retained even after the coating process (see CaP-Col in figure 3(a)). There was no remarkable difference in appearance, porous structure, and flexibility between the Col and CaP-Col sponges. This might be owing to the unique coating structure; the coating was composed of nano-sized CaP particles distributed over the sponge surface, as confirmed by the following FESEM and EDX analyses. The nano- and microstructural changes within the sponges due to the coating process were investigated by dividing the sponges into halves and analyzing their exposed surfaces (inner surfaces) along with their outer surfaces by FESEM and EDX. As shown in figure 3(b) (left), the inner and outer surfaces of the untreated Col sponges were smooth on a micrometer scale (see the magnified images in insets). On these surfaces, non-collagenous elements like Na and Cl were detected by FESEM-EDX (figure 4(a)). The FESEM-EDX and XRD results (figure 5(b)) suggest the presence of sodium chloride on the Col sponges, although cubic crystals characteristic of NaCl were not observed in their FESEM images (figure 3(b), left). On the CaP-Col and F-CaP-Col sponges (after the coating process), spherical nanoparticles with a diameter of 200–500 nm distributed over their inner and outer surfaces (figure 3(b), middle and right) were seen. These nanoparticles were composed of CaP, as indicated by the strong Ca and P peaks in the FESEM-EDX spectra of these sponges (figures 4(b) and 4(c)). The Na and Cl

peaks observed for the Col sponges disappeared for the CaP-Col and F-CaP-Col sponges. It is likely that sodium chloride contained in the Col sponges was dissolved and washed out from the sponges during the coating process.

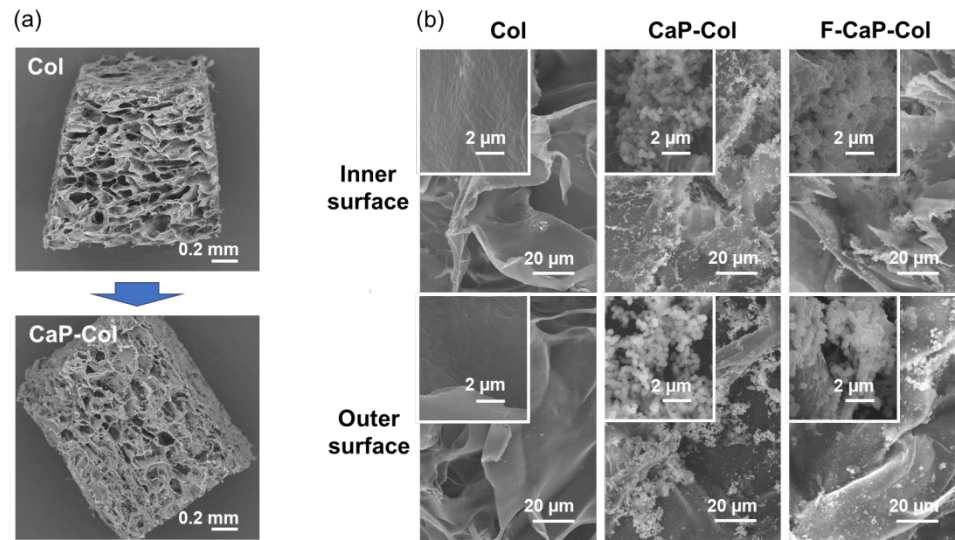


Figure 3. (a) SEM images (BSE mode) of the whole picture of the Col and CaP-Col sponges and (b) FESEM images (SE mode) of the inner (upper) and outer (lower) surfaces of the Col (left), CaP-Col (middle) and F-CaP-Col (right) sponges. Insets in (b) show higher magnification images. After the coating process, the sponges (CaP-Col and F-CaP-Col) were coated with nanoparticles on their inner and outer surfaces (b) with retaining their highly porous structure (a).

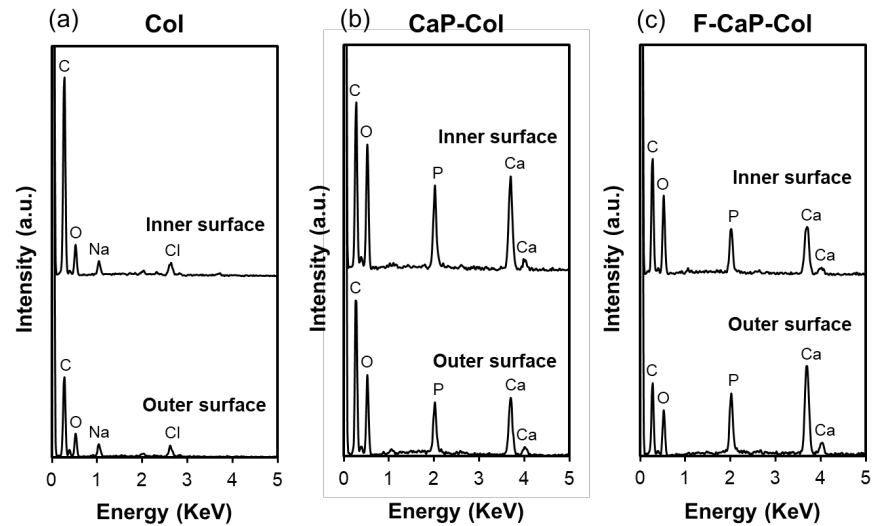


Figure 4. FESEM-EDX spectra of the inner (upper) and outer (lower) surfaces of the (a) Col, (b) CaP-Col and (c) F-CaP-Col sponges. After the coating process, the sponges (CaP-Col and F-CaP-Col) showed new peaks due to Ca and P in their FESEM-EDX spectra (b)(c).

The CaP formation and NaCl dissolution on the sponges during the coating process were confirmed by the FT-IR and XRD results, respectively. As shown in the FT-IR spectra (figure 5(a)), the Col sponges showed characteristic amide bands (amide I, amide II and amide III) present in collagen. In addition to these peaks ascribed to collagen, the CaP-Col and F-CaP-Col sponges showed an additional broad peak at approximately 1050 cm^{-1} representing PO_4^{3-} from CaP. In the XRD pattern (figure 5(b)), the Col sponges showed strong diffraction peaks attributed to crystalline NaCl along with a small peak from the silicon sample holder. The NaCl peaks disappeared for both the CaP-Col and F-CaP-Col sponges, being consistent with the EDX results shown in figure 4. Any other diffraction peaks were not detected in both the large (figure 5(b)) and small (figure 5(c)) angle regions.

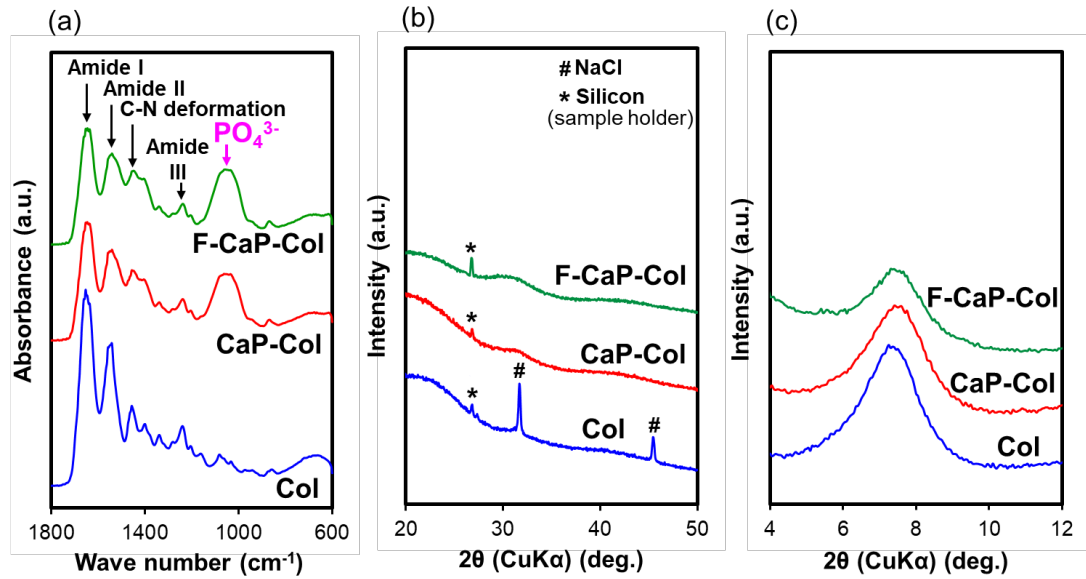


Figure 5. (a) FT-IR spectra and (b)(c) XRD patterns (b: large angle region, c: small angle region) of the Col, CaP-Col, and F-CaP-Col sponges. After the coating process, the sponges (CaP-Col and F-CaP-Col) showed a new IR peak ascribed to PO_4^{3-} (a), whereas peaks ascribed to crystalline CaPs were not detected in their XRD patterns (b)(c).

The CaP nanoparticles formed on the CaP-Col and F-CaP-Col sponges consisted of non-crystalline ACP. The CaP-Col and F-CaP-Col sponges showed a small halo at around 30° in their XRD patterns (figure 5(b)). Similar halo patterns have been reported for ACP [37]. Peaks ascribed to crystalline CaPs were not detected in either small angle (figure 5(c), main peak region of OCP) or large angle (figure 5(b), main peak region of apatite and β -TCP) region. Figure 6 shows the cross-sectional (a) TEM image, (b) SAED pattern, and (c) HAADF-STEM image of the CaP-Col sponges. Spherical nanoparticles were again observed in the TEM and HAADF-STEM images. The SAED pattern of the circular region in figure 6(a) showed neither diffraction spots nor Debye rings, suggesting that these CaP nanoparticles had an amorphous phase, which corresponds well to the XRD results (figures 5(b) and 5(c)). The STEM-EDX elemental mapping images of these CaP nanoparticles revealed homogenous distribution of

calcium, phosphorus, and oxygen over the nanoparticles (figure 6(d)). This result reconfirmed the FESEM-EDX results that the nanoparticle component was CaP (figures 4(b) and 4(c)).

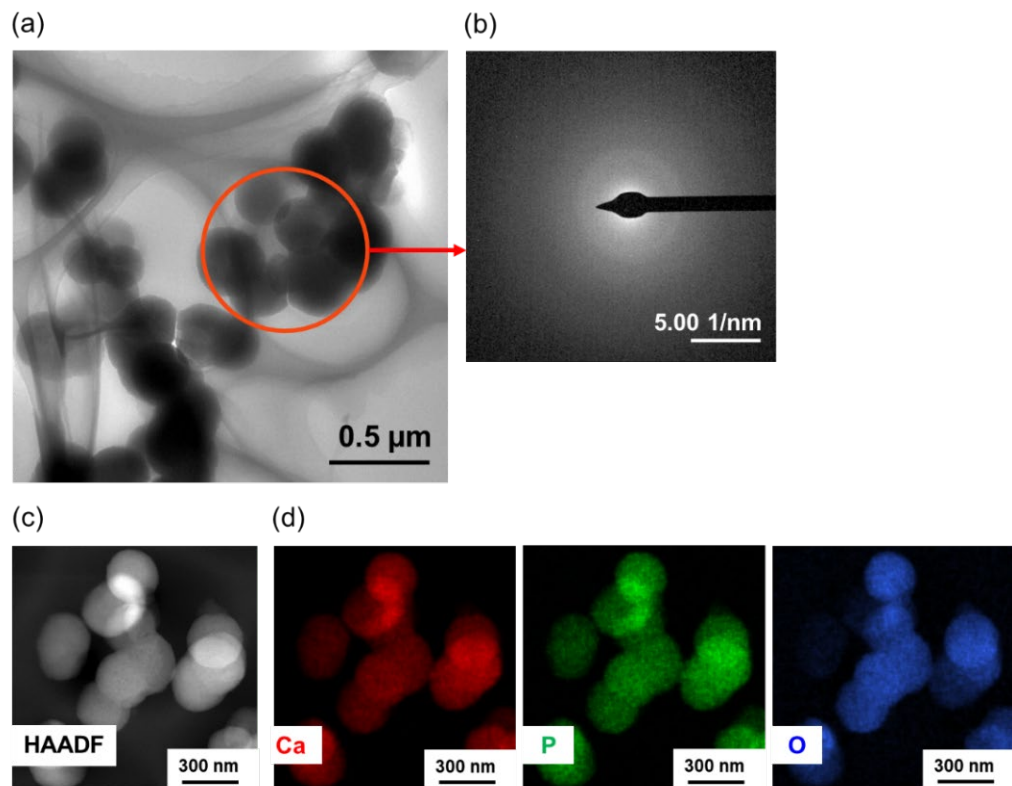


Figure 6. (a) TEM image, (b) SAED pattern obtained from the circled area in (a), (c) HAADF image, and (d) STEM-EDX elemental (Ca, P, O) mapping images of the cross-section of the CaP-Col sponge. The nanoparticles were composed of CaP (d) and had an amorphous structure (b).

According to the analytical results described above, the 3D porous collagen sponges were successfully coated with ACP nanoparticles on their inner as well as outer surfaces by the temperature-controlled coating process proposed in this study. There were no noticeable differences between the CaP-Col and F-CaP-Col sponges in figures 3–5 under the tested analytical conditions.

3.3. Putative reaction mechanism

The putative mechanism of ACP coating in the process proposed in this study can be described as follows. First, the collagen sponges were surface-modified by the oxygen gas plasma treatment. Due to this treatment, water wettability of the sponges was improved most likely due to the formation of hydrophilic functional groups on their surfaces [42]. The plasma-treated sponges were immersed fully in the cooled (4 °C) supersaturated CaP solution supplemented with carbonate ions (1st immersion step, see figure 1, left). In this step, the use of a vacuum degassing system in combination with a vent-cap tube assisted smooth penetration of the solutions within the porous sponges. During this step, the cooled CaP solution was metastable and did not induce visible CaP precipitation as shown in figure 2(a), although prenucleation CaP clusters [43, 44] may have existed in the solution. During the subsequent 2nd immersion step at 25 °C (see figure 1, right), the CaP solution warmed up quickly and induced aggregation of CaP clusters to form critical-sized amorphous CaP nuclei (homogeneous CaP precipitation) within 5 min as shown in figure 2(b) (lower row). The amorphous CaP nuclei formed in the CaP solution grew isotopically into spherical ACP nanoparticles 200–500 nm in diameter while retaining their amorphous phase after immersion for 24 h (figures 3-6). The high degree of supersaturation, relatively low temperature (compared with the body temperature), and high carbonate concentration of the CaP solution should be responsible for the inhibition of the amorphous-to-crystalline transformation [45]. The homogeneous CaP nucleation occurred throughout the CaP solution, therefore, the ACP nanoparticles formed even within the internal pores of the sponge resulting in *in situ* ACP precipitation within the sponges. The suspended ACP nanoparticles, with continuous shaking, attached to the inner and outer surfaces of the sponges due to the difference in their kinetics of motion. The ACP nanoparticles bound to the sponge surface so firmly that a reasonable number of them remained attached even after washing of the sponges (figure 3(b), middle and right).

Affinity interactions between CaP and functional groups on collagen might be involved in the firm binding of the CaP nanoparticles with the sponge surface. There might be a very thin CaP layer on the sponge's surface which acted as a binder for the CaP nanoparticles [37].

The increase in temperature of the CaP solution from 4 °C to 25 °C in the 2nd immersion step was a critical cue to induce homogeneous CaP nucleation in the solution. One reason for this phenomenon is that the mass transfer rate increases with increasing temperature of the CaP solution. Another reason is that the degree of supersaturation of CaP solutions with respect to CaPs increases as the solution temperature and pH increase under the tested conditions [31]. As described in Section 3.1, the pH of the CaP solution increased despite the pH-lowering effects due to the temperature rise and ACP precipitation [46]. This pH increase should be caused mainly by carbonate degassing from the solution because of the following reactions: [47] Carbonate ionic species in weakly alkaline solutions are in the form of HCO_3^- and CO_3^{2-} (H_2CO_3 is negligibly low in concentration), and are in equilibrium with gaseous CO_2 as shown by the equations (1)–(3). The increase in solution temperature from 4 °C to 25 °C results in decreased solubility of gaseous CO_2 in the CaP solution, which leads to carbonate degassing from the solution. As a result of this, Equation (1) shifts to the right, which decreases the aqueous CO_2 concentration in the solution. Consequently, equations (2) and (3) shift to the right resulting in increased pH due to the consumption of H_3O^+ in the solution.



3.4. Effect of ACP coating

The SBF test suggested that the ACP coating was effective in improving osteoconductivity of the collagen sponges. The ACP coating effect was verified by subjecting the CaP-Col and the Col (control) sponges to the SBF test. The SBF-test has long been used for predicting *in vivo* osteoconductivity of materials from their apatite-forming ability in SBF [38]. As shown in the FESEM images in figure 7(a), the surface morphology of the Col sponges remained unchanged, whereas that of the CaP-Col sponges changed remarkably after immersion in SBF for 7 d (compare with the lower left and lower middle images in figure 3(b)). After immersion in SBF, the nanoparticles existing on the pristine CaP-Col surfaces apparently disappeared and the surfaces were fully coated with a dense continuous layer having a nanoporous structure (see the inset in the right image in figure 7(a)) that is typical to bonelike apatite formed in SBF [48, 49]. This surface layer formed on the CaP-Col sponges was identified as apatite, as all the peaks detected in their XRD pattern were indexed to crystalline apatite (figure 7(b)). These results revealed that the CaP-Col sponges possess apatite-forming ability in SBF, although the Col sponges do not. It was therefore considered that the ACP nanoparticles did not dissolve completely in SBF but grew and crystalized eventually into apatite that is the most stable CaP phase in neutral solutions [31]. Apatite might be nucleated at the ACP-solution interface *via* polymorph transformation [50]. During this conversion process, OCP might be formed as an intermediate metastable phase, since SBF is supersaturated with respect to OCP as well as apatite [51]. A series of such reactions have also been reported to occur in the *in vivo* biomineralization process [29, 30].

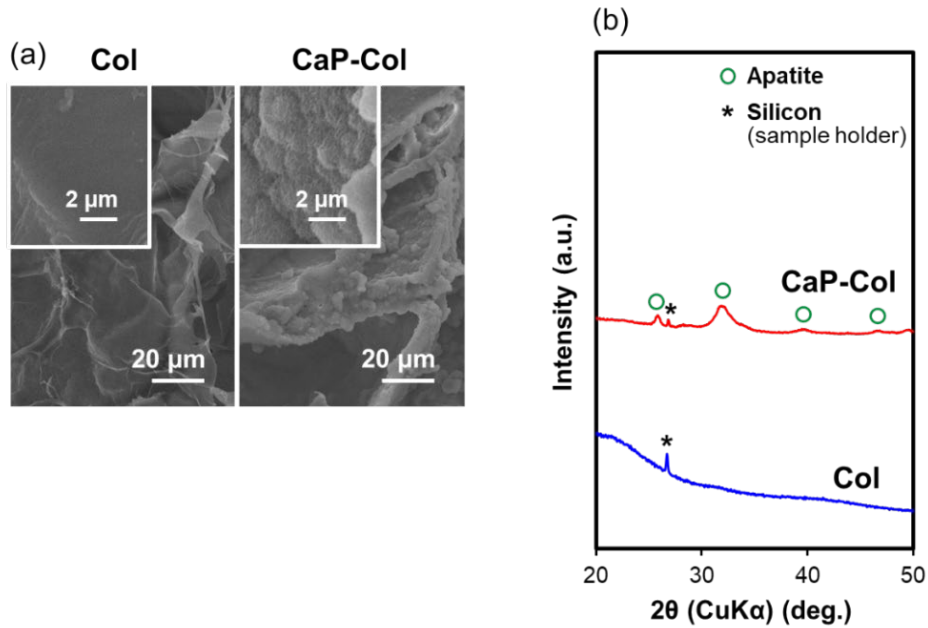


Figure 7. (a) FESEM images (SE mode) and (b) XRD patterns of the outer surfaces of the Col and CaP-Col sponges after immersion in SBF for 7 d. Insets in (a) show higher magnification images. The CaP-Col sponges with ACP coating formed apatite in SBF within 7 d whereas the Col sponges without coating did not.

Generally, materials with apatite-forming ability in SBF exhibit osteoconductivity *in vivo* [38]. This is because such materials form a bonelike layer on their surfaces in body environmental conditions, and integrate with the surrounding bone tissues through the interfacial apatite layer [38]. Therefore, the results obtained here strongly suggest better osteoconductivity of the CaP-Col sponges compared to the Col sponges.

3.5. Effect of bFGF supplementation

The temperature-controlled ACP coating process using the CaP solution supplemented with bFGF enabled the fabrication of ACP-coated collagen sponges with bFGF-release capability. Figure 8(a) shows bFGF-release profile of the F-CaP-Col sponges in the serum-free medium at 37 °C. As shown in this figure, the initial bFGF concentration in the medium (after

degassing) was 23.9 ± 4.3 ng/mL which decreased gradually with increasing incubation period up to 7 d. These values represent the concentration of ELISA-detectable bFGF, *i.e.*, bFGF that preserves its binding sites for a monoclonal antibody specific to human bFGF. According to previous reports, bFGF is highly unstable at body temperature [52], and free bFGF (10 ng/mL) added to a serum-free medium (37 °C) becomes barely detectable by ELISA within 1 d (0.3 ng/mL, 97% reduction in 1 d) [53]. In figure 8(a), the bFGF concentration in the medium decreased with time but not as much (24 % and 63 % reduction in 1 and 7 d, respectively) even at 37 °C. This result suggests that the F-CaP-Col sponges released bFGF in a sustained manner in the medium. It has been reported that certain types of proteins are immobilized within a CaP matrix through protein–CaP coprecipitation in supersaturated CaP solutions [54]. A similar coprecipitation reaction may have occurred in the coating process mentioned in this study, however, this is yet to be clarified. The mechanism behind the bFGF immobilization along with the state of bFGF immobilized on the F-CaP-Col sponges needs to be clarified in future studies.

The concentration of bFGF released from the F-CaP-Col sponges ranged between 9–24 ng/mL. In this concentration range, bFGF exhibits various biological activities including the activity to promote cell proliferation and bone tissue regeneration [55-57]. According to the results of cell proliferation assay, the bFGF released from the F-CaP-Col sponges retained its biological activity to promote cell proliferation. Figure 8(b) shows relative numbers of osteoblastic MC3T3-E1 cells (represented as absorbance at 450 nm) cultured for 3 and 7 d in the presence of the Col, CaP-Col, or F-CaP-Col sponges. A significant increase in relative cell numbers was found for the F-CaP-Col sponges with bFGF; the cell numbers were relatively larger for the F-CaP-Col sponges than for the Col and CaP-Col sponges. The bFGF released from the F-CaP-Col sponges could be responsible for the enhanced cell proliferation.

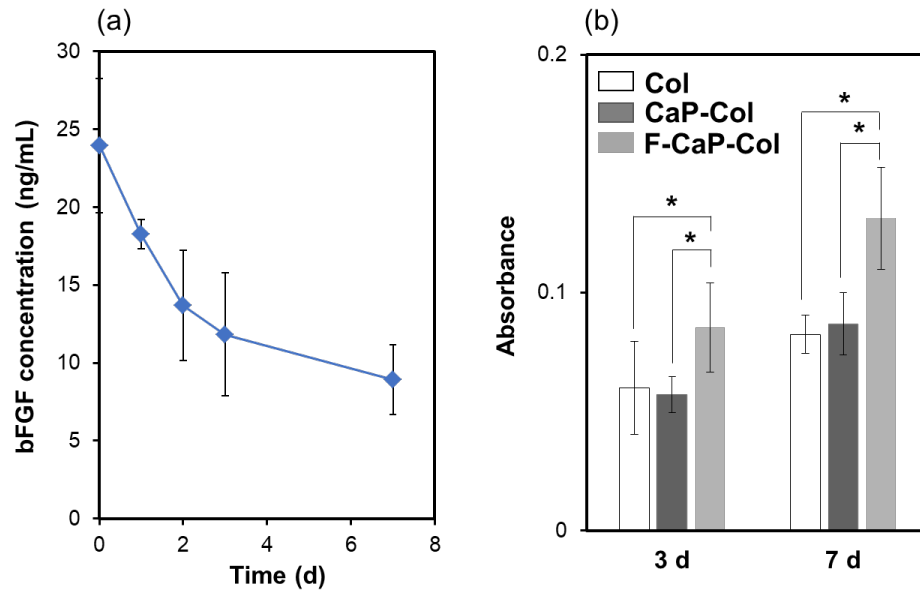


Figure 8. (a) Release profile of bFGF (concentration measured by ELISA) from the F-CaP-Col sponges in the serum-free medium ($n=3$, mean \pm SD) and (b) relative number (absorbance at 450 nm) of MC3T3-E1 cells cultured in the serum-free medium with Col, CaP-Col, and F-CaP-Col sponges for 3 and 7 d ($n=6$, mean \pm SD). The F-CaP-Col sponges released bFGF in the medium in a sustained manner (a), and enhanced cell proliferation compared to the Col and CaP-Col sponges (b).

3.6. Potential of the process and the resulting sponges to be used in bone tissue engineering

This study established the temperature-controlled ACP coating process on the 3D porous collagen sponges using supersaturated CaP solutions. In this process, 3D porous sponges were coated on their inner and outer surfaces by ACP through *in situ* ACP precipitation within the sponges *via* a 2-step temperature control of the CaP solution (figure 1). This coating process involves highly safe sources only. We used a clinically approved bioresorbable artificial dermis as the collagen sponge and a clinically approved drug (for pressure ulcers and other skin ulcers) as the bFGF source. The source solutions (1)–(4) used for the coating process

have ion concentrations equivalent to those of injection solutions used in clinical practice. The source solution (6) was a clinically approved physiological saline, and this was mixed with bFGF to prepare the source solution (5). This process involves any other sources; hence it is well-suited for clinical applications. In addition, this process is performed under mild conditions using versatile instruments. Owing to the mild conditions, unstable cytokine bFGF could be immobilized on the sponges during the process of ACP coating without causing deactivation of bFGF (figure 8(b)). Further, it would be possible to immobilize other bioactive molecules besides bFGF on the sponges using the process developed in this study. That is, the present process has potential for further customization of the ACP-coated sponges by selecting the best set of bioactive molecules to be used in bone tissue engineering. These are potential advantages of the present process over other ACP fabrication processes including a conventional precipitation process, sol-gel process, flame spray process, and mechano-chemical process [45].

The resulting ACP-coated sponges with bFGF-release capability are expected to be useful as bone tissue engineering scaffolds. The fabricated ACP coating was composed of fine nanoparticles which were much smaller than the sponge pore-size and scattered over the sponge surface (figures 3(b), middle and right). Hence, the ACP-coated collagen sponges retained their highly porous structure (figure 3(a)) along with their intrinsic flexibility even after the coating process. The porous structure should allow transportation of nutrients and metabolites, cell infiltration, and blood vessel ingrowth within the sponges. The ACP-coated sponges should be able to undergo the biomineralization process to form a bone like apatite layer on their surfaces as suggested by the SBF test (figure 7). The ACP- and apatite-coated collagen sponges would provide a suitable environment for new bone formation owing to their osteoconductivity [16-18]. In addition, bone formation might be enhanced by the therapeutic effect of bFGF released

from the sponges. Further *in vitro* and *in vivo* studies are needed to evaluate the biological function of the ACP-coated sponges as scaffolds for use in bone tissue engineering.

4. Conclusion

Three-dimensional porous collagen sponges coated with ACP nanoparticles on their inner as well as outer surfaces were fabricated through *in situ* ACP precipitation within the sponges by the temperature-controlled coating process using the supersaturated CaP solution. The SBF test suggested osteoconductivity of the resulting ACP-coated sponges. Further, ACP-coated sponges with immobilized cytokine bFGF were fabricated using the CaP solution supplemented with bFGF. The bFGF-immobilized ACP-coated sponges showed sustained release of bFGF into the medium and enhanced the proliferation of the osteoblastic MC3T3-E1 cells. The coating process developed in the present study and the fabricated sponges would be useful in bone tissue engineering and would benefit from further *in vitro* and *in vivo* studies.

Acknowledgements

This study was supported by JSPS KAKENHI JP18F18106. We thank Ms. Ikuko Sakamaki, Dr. Ding Wuxiao, Dr. N. Yoshizawa, and Mr. N. Saito from AIST for their technical support.

References

1. A. El-Ghannam, Bone reconstruction: from bioceramics to tissue engineering, *Expert Rev. Med. Devices* 2 (2005) 87–101.
2. T. Miyata, T. Taira, Collagen engineering for biomaterial use, *Clin. Mater.* 9 (1992) 139–148.

3. K.I. Clarke, S.E. Graves, A.T.C. Wong, J.T. Triffitt, M.J.O. Francis, J.T. Czernuszka, Investigation into the formation and mechanical properties of a bioactive material based on collagen and calcium phosphate, *J. Mater. Sci. Mater. Med.* 4 (1993) 107–110.
4. M. Kikuchi, S. Itoh, S. Ichinose, K. Shinomiya, J. Tanaka, Self-organization mechanism in a bone-like hydroxyapatite/collagen nanocomposite synthesized in vitro and its biological reaction in vivo, *Biomaterials* 22 (2001) 1705–1711.
5. Y. Honda, K. Kamakura, S. Sasaki, O. Suzuki, Formation of bone-like apatite enhanced by hydrolysis of octacalcium phosphate crystals deposited in collagen matrix, *J. Biomed. Mater. Res. B Appl. Biomater.* 80 (2007) 281–289.
6. A.A. Al-Munajjed, F.J. O'Brien, Influence of a novel calcium-phosphate coating on the mechanical properties of highly porous collagen scaffolds for bone repair, *J. Mech. Behav. Biomed. Mater.* 2 (2009) 138–146.
7. N. Nassif, F. Gobeaux, J. Seto, E. Belamie, P. Davidson, P. Panine, G. Mosser, P. Fratzl, M.G. Marie-Guille. Self-assembled collagen-apatite matrix with bone-like hierarchy, *Chem. Mater.* 22 (2010) 3307–3309.
8. A. Ibara, H. Miyaji, B. Fugetsu, E. Nishida, H. Takita, S. Tanaka, T. Sugaya, M. Kawanami, Osteoconductivity and biodegradability of collagen scaffold coated with nano- β -TCP and fibroblast growth factor 2. *J. Nanomater.* 2013 (2013) 639502.
9. C.A. Bertran, L.J.M. Allegretti, S. Bertazzo, Synthesis of calcium phosphate nanoparticles in collagen medium, *Macromol. Symp.* 253 (2007) 77–81.
10. S. Murakami, H. Miyaji, E. Nishida, K. Kawamoto, S. Miyata, H. Takita, T. Akasaka, B. Fugetsu, T. Iwanaga, H. Hongo, N. Amizuka, T. Sugaya, M. Kawanami, Dose effects of beta-tricalcium phosphate nanoparticles on biocompatibility and bone conductive ability of three-dimensional collagen scaffolds, *Dent. Mater. J.* 36 (2017) 573–583.

11. A.J. Nathanael, A. Oyane, M. Nakamura, I. Sakamaki, E. Nishida, Y. Kanemoto, H. Miyaji, In Vitro and in vivo analysis of mineralized collagen-based sponges prepared by a plasma- and precursor-assisted biomimetic process, *ACS Appl. Mater. Interf.* 9 (2017) 22185–22194.
12. A. Kouketsu, K. Matsui, T. Kawai, Y. Ezoe, T. Yanagisawa, A. Yasuda, T. Takahashi, S. Kamakura, Octacalcium phosphate collagen composite stimulates the expression and activity of osteogenic factors to promote bone regeneration, *J. Tissue Eng. Regen. Med.* 14 (2020) 99–107.
13. C. Du, F.Z. Cui, W. Zhang, Q.L. Feng, X.D. Zhu, K. de Groot, Formation of calcium phosphate/collagen composites through mineralization of collagen matrix, *J. Biomed. Mater. Res.* 50 (2000) 518–527.
14. K. Yamauchi, T. Goda, N. Takeuchi, H. Einaga, T. Tanabe, Preparation of collagen/calcium phosphate multilayer sheet using enzymatic mineralization, *Biomaterials* 25 (2004) 5481–5489.
15. A. La Fontaine, A. Zavgorodniy, H. Liu, R. Zheng, M. Swain, J. Cairney, Atomic-scale compositional mapping reveals Mg-rich amorphous calcium phosphate in human dental enamel. *Sci. Adv.* 2 (2016) e1601145.
16. B.M. Whited, D. Skrtic, B.J. Love, A.S. Goldstein, Osteoblast response to zirconia-hybridized pyrophosphate-stabilized amorphous calcium phosphate, *J. Biomed. Mater. Res. A* 76 (2006) 596–604.
17. S. Yokota, N. Nishiwaki, K. Ueda, T. Narushima, H. Kawamura, T. Takahashi, Evaluation of thin amorphous calcium phosphate coatings on titanium dental implants deposited using magnetron sputtering, *Implant Dent.* 23 (2014) 343–350.
18. K. Masamoto, S. Fujibayashi, T. Yabutsuka, T. Hiruta, B. Otsuki, Y. Okuzu, K. Goto, T. Shimizu, Y. Shimizu, C. Ishizaki, K. Fukushima, T. Kawai, M. Hayashi, K. Morizane,

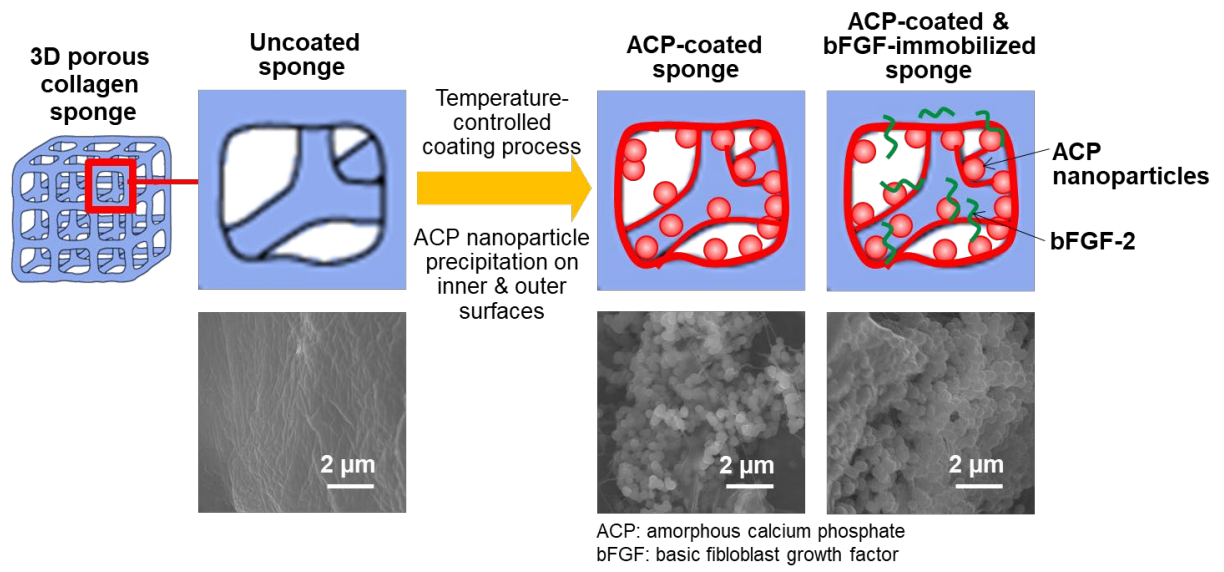
- T. Kawata, M. Imamura, S. Matsuda, In vivo and in vitro bioactivity of a “precursor of apatite” treatment on polyetheretherketone, *Acta Biomater.* 91 (2019) 48–59.
19. G. Balasundaram, M. Sato, T.J. Webster, Using hydroxyapatite nanoparticles and decreased crystallinity to promote osteoblast adhesion similar to functionalizing with RGD, *Biomaterials* 27 (2006) 2798–2805.
20. I. Kim, H.J. Kim, H.M. Kim, Array of amorphous calcium phosphate particles improves cellular activity on a hydrophobic surface, *J. Biomed. Mater. Res. B Appl. Biomater.* 93 (2010) 113–121.
21. J.R. Popp, K.E. Laflin, B.J. Love, A.S. Goldstein, In vitro evaluation of osteoblastic differentiation on amorphous calcium phosphate-decorated poly(lactic-co-glycolic acid) scaffolds, *J. Tissue Eng. Regen. Med.* 5 (2011) 780–789.
22. F.N. Syed-Picard, T. Jayaraman, R.S. Lam, E. Beniash, C. Sfeir. Osteoinductivity of calcium phosphate mediated by connexin 43, *Biomaterials* 34 (2013) 3763–3774.
23. X. Niu, Z. Liu, F. Tian, S. Chen, L. Lei, T. Jiang, Q. Feng, Y. Fan, Sustained delivery of calcium and orthophosphate ions from amorphous calcium phosphate and poly(L-lactic acid)-based electrospinning nanofibrous scaffold, *Sci. Rep.* 7 (2017) 45655.
24. M. Nagano, T. Nakamura, T. Kokubo, M. Tanahashi, M. Ogawa, Differences of bone bonding ability and degradation behaviour in vivo between amorphous calcium phosphate and highly crystalline hydroxyapatite coating, *Biomaterials* 17 (1996) 1771–1777.
25. J.R. Popp, K.E. Laflin, B.J. Love, A.S. Goldstein, Fabrication and characterization of poly(lactic-co-glycolic acid) microsphere/amorphous calcium phosphate scaffolds, *J. Tissue Eng. Regen. Med.* 6 (2012) 12–20.

26. F. Nudelman, K. Pieterse, A. George, P.H. Bomans, H. Friedrich, L.J. Brylka, P.A. Hilbers, G. de With, N.A. Sommerdijk, The role of collagen in bone apatite formation in the presence of hydroxyapatite nucleation inhibitors, *Nat. Mater.* 9 (2010) 1004–1009.
27. S. Boonrungsiman, E. Gentleman, R. Carzaniga, N.D. Evans, D.W. McComb, A.E. Porter, M.M. Stevens, The role of intracellular calcium phosphate in osteoblast-mediated bone apatite formation, *Proc. Natl Acad. Sci. USA* 109 (2012) 14170–14175.
28. A. Lotsari, A.K. Rajasekharan, M. Halvarsson, M. Andersson, Transformation of amorphous calcium phosphate to bone-like apatite, *Nat. Commun.* 9 (2018) 4170.
29. J. Mahamid, A. Sharir, L. Addadi, S. Weiner, Amorphous calcium phosphate is a major component of the forming fin bones of zebrafish: Indications for an amorphous precursor phase, *Proc. Natl. Acad. Sci. USA* 105 (2008) 12748–12753.
30. E. Beniash, R.A. Metzler, R.S. Lam, P.U. Gilbert, Transient amorphous calcium phosphate in forming enamel, *J. Struct. Biol.* 166 (2009) 133–143.
31. J.C. Elliot, *Structure and chemistry of the apatites and other calcium orthophosphates*, first ed., Elsevier, 1994.
32. J. Mahamid, A. Sharir, D. Gur, E. Zelzer, L. Addadi, S. Weiner, Bone mineralization proceeds through intracellular calcium phosphate loaded vesicles: a cryo-electron microscopy study, *J. Struct. Biol.* 174 (2011) 527–535.
33. X. Huang, D. Yang, W. Yan, Z. Shi, J. Feng, Y. Gao, W. Weng, S. Yan, Osteochondral repair using the combination of fibroblast growth factor and amorphous calcium phosphate/poly(L-lactic acid) hybrid materials, *Biomaterials.*, 28 (2007) 3091–3100.
34. A.M. Ambrosio, J.S. Sahota, Y. Khan, C.T. Laurencin, A novel amorphous calcium phosphate polymer ceramic for bone repair: I. Synthesis and characterization, *J. Biomed. Mater. Res.* 58 (2001) 295–301.

35. T. Santoso, N.K. Djauharie, Kamizar, W. Ahdi, F.D.E. Latief, E. Suprastiwi, Carboxymethyl Chitosan/Amorphous Calcium Phosphate and Dentin Remineralization, *J. Int. Dent. Med. Res.* 12 (2019) 84–87.
36. A. Oyane, H. Araki, Y. Sogo, A. Ito, H. Tsurushima, Spontaneous assembly of DNA–amorphous calcium phosphate nanocomposite spheres for surface-mediated gene transfer, *Cryst. Eng. Comm.* 15 (2013) 4994–4997.
37. A. Oyane, H. Araki, M. Nakamura, Y. Shimizu, Q.T.H. Shubhra, A. Ito, H. Tsurushima, Controlled superficial assembly of DNA–amorphous calcium phosphate nanocomposite spheres for surface-mediated gene delivery, *Coll. Surf. B Biointerf.* 141 (2016) 519–527.
38. T. Kokubo, H. Takadama, How useful is SBF in predicting in vivo bone bioactivity? *Biomaterials* 27 (2006) 2907–2915.
39. Y.R. Yun, J.E. Won, E. Jeon, S. Lee, W. Kang, H. Jo, J.H. Jang, U.S. Shin, H.W. Kim, Fibroblast growth factors: biology, function, and application for tissue regeneration, *J. Tissue Eng.* 2010 (2010) 218142.
40. K. Hori, A. Osada, T. Isago, H. Sakurai, Comparison of contraction among three dermal substitutes: Morphological differences in scaffolds, *Burns* 43 (2017) 846–851.
41. Q.T.H. Shubhra, A. Oyane, H. Araki, M. Nakamura, H. Tsurushima, Calcium phosphate nanoparticles prepared from infusion fluids for stem cell transfection: process optimization and cytotoxicity analysis, *Biomater. Sci.* 5 (2017) 972–981.
42. E.M. Liston, L. Martinu, M.R. Wertheimer, Plasma surface modification of polymers for improved adhesion: a critical review, *J. Adhesion Sci. Tech.* 7 (1993) 1091–1127.
43. K. Onuma, A. Ito, Cluster Growth Model for Hydroxyapatite, *Chem. Mater.* 10 (1998) 3346–3351.

44. A. Dey, P.H. Bomans, F.A. Müller, J. Will, P.M. Frederik, G. de With, N.A. Sommerdijk, The role of prenucleation clusters in surface-induced calcium phosphate crystallization, *Nat. Mater.* 9 (2010) 1010–1014.
45. C. Combes, C. Rey, Amorphous calcium phosphates: Synthesis, properties and uses in biomaterials, *Acta Biomater.* 6 (2010) 3362–3378.
46. V. Čadež, I. Erceg, A. Selmani, D. Domazet Jurašin, S. Šegota, D.M. Lyons, D. Kralj, M.D. Sikirić, Amorphous calcium phosphate formation and aggregation process revealed by light scattering techniques, *Crystals* 8 (2018) 254.
47. P. Habibovic, F. Barre`re, C.A. van Blitterswijk, K. de Groot, P. Layrolle, Biomimetic hydroxyapatite coating on metal implants, *J. Am. Ceram. Soc.* 85 (2002) 517–522.
48. H.M. Kim, K. Kishimoto, F. Miyaji, T. Kokubo, T. Yao, Y. Suetsugu, J. Tanaka, T. Nakamura, Composition and structure of the apatite formed on PET substrates in SBF modified with various ionic activity products, *J. Biomed. Mater. Res.* 46 (1999) 228–235.
49. H. Mutsuzaki, Y. Yokoyama, A. Ito, A. Oyane, Formation of apatite coatings on an artificial ligament using a plasma- and precursor-assisted biomimetic process, *Int. J. Mol. Sci.* 14 (2013) 19155–19168.
50. S. Jiang, H. Pan, Y. Chen, X. Xu, R. Tang, Amorphous calcium phosphate phase-mediated crystal nucleation kinetics and pathway, *Faraday Discuss.* 179 (2015) 451–461.
51. S. Sakai, T. Anada, K. Tsuchiya, H. Yamazaki, H.C. Margolis, O. Suzuki, Comparative study on the resorbability and dissolution behavior of octacalcium phosphate, β -tricalcium phosphate, and hydroxyapatite under physiological conditions, *Dent. Mater. J.* 35 (2016) 216–224.
52. G. Chen, D.R. Gulbranson, P. Yu, Z. Hou, J.A. Thomson, Thermal stability of fibroblast growth factor protein is a determinant factor in regulating self-renewal, differentiation, and reprogramming in human pluripotent stem cells, *Stem Cells* 30 (2012) 623–630.

53. A. Oyane, H. Araki, M. Nakamura, Y. Aiki, K. Higuchi, A. Pyatenko, M. Adachid, Y. Ito, Controlled release of basic fibroblast growth factor from a water-floatable polyethylene nonwoven fabric sheet for maintenance culture of iPSCs, *RSC Adv.* 10 (2020) 95–104.
54. A. Oyane, M. Uchida, K. Onuma, A. Ito, Spontaneous growth of a laminin-apatite nanocomposite in a metastable calcium phosphate solution, *Biomaterials* 27 (2006) 167–175.
55. A.Q. Zheng, J. Xiao, J. Xie, P.P. Lu, X. Ding, bFGF enhances activation of osteoblast differentiation and osteogenesis on titanium surfaces via PI3K/Akt signaling pathway, *Int. J. Clin. Exp. Pathol.* 9 (2016) 4680–4692.
56. H. Tsurushima, A. Marushima, K. Suzuki, A. Oyane, Y. Sogo, K. Nakamura, A. Matsumura, A. Ito, Enhanced bone formation using hydroxyapatite ceramic coated with fibroblast growth factor-2, *Acta Biomater.* 6 (2010) 2751–2759.
57. J.B. Park, Effects of the combination of fibroblast growth factor-2 and bone morphogenetic protein-2 on the proliferation and differentiation of osteoprecursor cells, *Adv. Clin. Exp. Med.* 23 (2014) 463–467.



Graphical abstract